

THE NONLINEAR MAGNETIC CASCADE¹

JASON MARON AND STEVEN COWLEY

Blackett Laboratory, Imperial College of Science, Technology and Medicine, Prince Consort Road, London SW7 2BZ, UK;
maron@tapir.caltech.edu, steve.cowley@ic.ac.uk

AND

JAMES McWILLIAMS

Department of Atmospheric Sciences, University of California at Los Angeles, Los Angeles, CA 90024; jcm@ucar.edu

Received 2003 April 26; accepted 2003 October 6

ABSTRACT

The Galactic magnetic field has an energy density comparable to that of the interstellar medium turbulence and a coherence spanning the Galaxy. It is not known if this field was formed before, during, or after the Galaxy. However, it is often assumed to originate from a turbulent dynamo process. We investigate the early stages of a Galactic dynamo when the dynamics is well approximated by homogeneous turbulence. Our simulations show that homogeneous magnetized turbulence with large Prandtl number yields magnetic energy at the small, resistive scale rather than at the Galactic scale. Thus, additional phenomena—perhaps helicity generated from Galactic rotation, stratification, and the differential rotation of the disk—are needed to explain the observed field. We simulate the growth of magnetic energy in forced nonhelical turbulence from an initially weak value until it saturates with the same energy density as the turbulence. When the field is dynamically weak, the simulations agree with the kinematic theory. In the long-term saturated state, the magnetic field is strong enough to modify the turbulence. This is the magnetohydrodynamic (MHD) analog of the Kolmogorov problem for hydrodynamic turbulence. The nature of the back-reaction is to neutralize the net shear (stretching) in small-scale eddies that are less energetic than the magnetic field. Only the forcing-scale eddies remain energetic enough to shear and cascade the magnetic field. The magnetic field at all scales therefore forward-cascades at the forcing timescale through spectrally nonlocal interactions with the forcing-scale eddies. Furthermore, the magnetic field folds into a reduced-tension state where field-line curvature anticorrelates with intensity. Direct consequences of these statements are that the magnetic spectrum is largely independent of viscosity and that the magnetic energy is located at the small, resistive scale.

Subject headings: ISM: magnetic fields — methods: numerical — MHD — turbulence

1. INTRODUCTION

Microgauss magnetic fields are observed in spiral galaxies and between galaxies in clusters (Zweibel & Heiles 1997; Kronberg 1994; Vallee 1998; Beck et al. 1996). In cluster plasmas the fields have coherence lengths of up to 10 kpc (Taylor et al. 1999; Carilli & Taylor 2002). In galaxies the magnetic fields are ordered over the whole galaxy and have energy densities comparable to the turbulent energy density. It is not known if the fields originated before, during, or after galaxy formation. Most current research centers around dynamo theories where turbulent motions amplify the field from an initial weak seed field to its present strength and structure (Ruzmaikin et al. 1988; Kulsrud 1999; Zweibel & Heiles 1997; Beck et al. 1996). Indeed, some kind of dynamo seems to be the most plausible explanation of the observations. However, despite considerable progress over 40 years, the dynamo theory is not complete and thus the history of Galactic and extragalactic fields is uncertain. The Galactic dynamo (if it exists) differs from the more familiar solar dynamo (Mestel 1999) and geodynamo (Glatzmaier & Roberts 1995) in two key ways. First, the disk geometry of the Galaxy clearly affects the magnetic field dynamics. Second, the ratio of viscosity to resistivity, the magnetic Prandtl number (Pr), is of order 10^{14} in the warm partially ionized interstellar medium

but only $1-10^{-2}$ in the solar convection zone. The Prandtl number of a typical protogalactic plasma is also large ($Pr \sim 10^{19}$). In this paper we show that high Prandtl number dynamos are profoundly different from low Prandtl number dynamos.

The Galactic spatial scales and their associated timescales suggest a *possible* scenario for field growth. Elements of this scenario are suggested by the work of Kulsrud & Anderson (1992) and, particularly for the later stages (stage 3; see below), Field, Blackman, & Chou (1999). We take this scenario as a framework for discussion and not as proven. Indeed our calculations already expose flaws in the scenario. First, consider the important space scales and timescales from the largest to the smallest. The Galaxy itself is about 10^{10} yr old, 10–15 kpc ($=\lambda_g$) across, and rotates with velocity ~ 200 km s^{-1} once every 2×10^8 yr. Supernovae produce random velocities of order 10 km s^{-1} on a scale of 100 pc ($=\lambda_p$) and with timescales of order 10^7 yr. Approximately 5%–15% of the kinetic energy at the supernova scale is helical (Moffatt 1978). Without a magnetic field the kinetic energy cascades to small viscous scales λ_ν , where $\lambda_\nu \sim 0.1 - 0.01$ pc. The viscous eddies turn over on a timescale $\tau_\nu \sim 10^5$ yr. Finally, the smallest scale is the resistive scale λ_η , which is typically 10^8-10^{10} cm, truly negligibly small. The interstellar medium is, of course, very inhomogeneous: we have taken values of the physical parameters from the warm partially ionized medium. For reference the typical values of these

¹ For Edward Burns, 1970–2002.

TABLE 1
GALACTIC TURBULENCE PARAMETERS

Quantity	Galactic	Protogalactic
Magnetic coherence scale λ_g (cm)	10^{22}	...
Forcing scale λ_f (cm)	10^{20} – 10^{21}	10^{23}
Forcing velocity v_f (cm s $^{-1}$)	10^6	10^7
Viscous scale λ_ν (cm)	10^{17}	10^{22}
Resistive scale λ_η (cm)	10^8 – 10^{10}	10^{12}
Viscosity ν (cm 2 s $^{-1}$)	10^{20} – 10^{21}	10^{29}
Magnetic diffusivity η (cm 2 s $^{-1}$)	10^7	10^{10}
Prandtl number Pr	10^{14}	10^{19}
Neutral free path λ_{nm} (cm)	10^{15}	...
Ion free path λ_{ii} (cm)	10^{13}	10^{22}
Temperature T (K)	10^4	10^7
Proton density n (cm $^{-3}$)	1	10^{-2}

parameters are given in Table 1. It should be noted that although conditions in the other phases of the interstellar medium are quite different, the magnetic Reynolds number and Prandtl number are large in all phases.

We assume that the initial seed field is very weak. Such weak fields can be made in many different ways (see, for instance, Gnedin, Ferrara, & Zweibel 2000, who find that fields of order 10^{-18} G can be made in shocks during the reionization phase of structure formation). Thus, we need about 30 e -foldings to reach the present Galactic field strength of 3×10^{-6} G. We divide the growth of Galactic fields into three stages:

1. *The kinematic small-scale field dynamo.*—During this stage the field is too weak to affect the velocity at any scale. Since the eddies at the viscous scale turn over the fastest, they amplify the field at first. Therefore, the exponential growth time is approximately 10^5 yr in our Galaxy. Since the viscous-scale eddies have negligible helicity, the field growth is driven by homogeneous isotropic turbulence. This growth was first predicted by Batchelor (1950) and later by Kazantsev (1968), who also investigated the structure of the field, and still more recently Kulsrud & Anderson (1992) gave a spectral theory of the process. In the 1990s the kinematic theory was considerably refined (Schekochihin, Boldyrev, & Kulsrud 2002a; Chertkov et al. 1999), and it is well understood. Much of what is understood comes from the short correlation time kinematic model in which the velocity correlation time is assumed infinitesimal. The important features of the magnetic field evolution in this model are as follows: First, the magnetic spectrum $E_b(k, t)$ rises as $k^{3/2}$ at all k much less than the peak, k_p . Second, for $k \ll k_p$, $E_b(k, t)$ grows as $\exp(3\gamma t/4)$ at fixed k with γ roughly the turnover rate of the viscous-scale eddies. The peak wavenumber, k_p , increases as $k_p \propto \exp(3\gamma t/5)$ until it reaches, and remains at, the resistive scale [$k_\eta \sim 1/(\lambda_\eta) \sim (\gamma/\eta)^{1/2}$, with η the resistivity]. Finally, the magnetic field is in a folded state (Schekochihin et al. 2002c), where the variation of \mathbf{B} along itself ($(|\mathbf{B} \cdot \nabla \mathbf{B}|^2)$) is much smaller than the variation of B across itself ($(|\mathbf{B} \times (\nabla \times \mathbf{B})|^2)$). All these features of the kinematic phase evolution are seen, at least qualitatively, in the early stages of our simulations. Clearly, the field predicted by the small-scale field dynamo is on scales much smaller than the observed Galactic field. Stage 1 is necessarily a transitory stage. When the magnetic field energy becomes comparable to the energy in the viscous-scale eddies, the kinematic stage (stage 1) ends. In the Galaxy this corresponds to a magnetic field strength of approximately $0.1 \mu\text{G}$.

2. *Approach to equipartition.*—While magnetic forces at the end of stage 1 can change the viscous-scale flows, they are not strong enough to affect the more energetic larger scale motions. The strain of these larger scale motions continues to amplify the field. One would expect that these scales act on the field in a way similar to the viscous-scale eddies in stage 1, but on a slower timescale. As the field grows, more of the velocity spectrum is affected by the magnetic forces (see § 5). Eventually on a timescale of a few large eddy turnover times the magnetic energy becomes of order the kinetic energy of the large stirring-scale motions. In the Galaxy the timescale for this is the supernova stirring time, roughly 10^7 yr. On this timescale the Galactic rotation and the helical component of the turbulence have negligible effect. The growth up to the end of this stage could alternatively have taken place in the protogalactic plasma where rotation is negligible.

This stage is poorly understood and is the main subject of this paper. Meneguzzi, Frisch, & Pouquet (1981) computed the turbulent amplification of magnetic fields in a $\text{Pr} \sim 1$ plasma. They showed that without helicity the magnetic energy grew until it saturated at about 15% of the kinetic energy. Their magnetic and kinetic spectra resemble our lower resolution, $\text{Pr} \sim 1$, computations (for example, see Fig. 13 below). There is no evidence from these simulations (or our own) that there is energy equipartition scale by scale. In fact, in the $\text{Pr} \gg 1$ case, most of the magnetic energy is in the scales between the viscous and (smaller) resistive scale. However, almost none of the kinetic energy is contained in the subviscous scales. The saturated magnetic and kinetic energies are very nearly equal at $\text{Pr} \gg 1$.

Recently there has been considerable interest in simulating Alfvén wave turbulence (Maron & Goldreich 2001; Kinney & McWilliams 1998; Cho & Vishniac 2000a, 2000b; Muller & Biskamp 2000). Identical magnetic and kinetic power-law spectra ($k^{-\alpha}$ with $\alpha = 1.5 - 1.7$) are seen. These simulations start with magnetic energy on the large scale (particularly in the uniform field component) that is stronger or of order the kinetic energy of the forcing scale. The uniform field component cannot be changed by the flow and thus remains strong throughout. Dynamo simulations must, of course, start with small fields (in the uniform and non-uniform field). The spectra we generate are not like the Alfvén wave spectra; specifically, they are dominated by small-scale field. Clearly, the Alfvén wave turbulence model does not describe the field at the end of stage 2. It is, however, of considerable interest in describing the turbulence in the interstellar medium when a large-scale field is already present.

In summary, at the end of stage 2 the magnetic energy is of order the kinetic energy of the forcing motions and most of the magnetic energy is in the subviscous scales.

3. *Large-scale field growth.*—The final stage of the magnetic field evolution is growth of the field on the largest scale, the Galactic scale. It is believed (Pouquet et al. 1976; Meneguzzi, Frisch, & Pouquet 1981; Field et al. 1999; Brandenburg 2001) that the helicity ($\langle \mathbf{v} \cdot \nabla \times \mathbf{v} \rangle$) of the turbulence at the supernova scale plays a key role in this “inverse cascade.” Indeed, Field, Blackman, & Chou (1999) have argued that this stage is very similar to the kinematic (α - ω) mean field dynamo (Parker 1979; Moffatt 1978; Ruzmaikin, Shukurov, & Sokoloff 1988).

The estimated timescale for the mean field dynamo in the Galaxy is 2×10^8 yr (Field et al. 1999; Kulsrud 1999). This timescale is controlled by the slow rotation of the Galaxy that gives ω and drives the helicity in the turbulence to give α . The fraction of the turbulent energy in the Galaxy that is helical is about 5%–15%. The crucial question is how the mean

magnetic field grows in the presence of small-scale fields generated by the more vigorous nonhelical flows. Indeed there is an ongoing debate about the effect of small-scale fields on the mean field dynamo: several authors have claimed a quenching (suppression) of the alpha effect (Cattaneo & Hughes 1996; Gruzinov & Diamond 1994; Bhattacharjee & Yuan 1995). Most of these discussions focus on the evolution of the magnetic helicity $\langle \mathbf{A} \cdot \mathbf{B} \rangle$, since the large-scale field that is generated by the α - ω dynamo is helical. It is not clear, however, that the observed fields have significant magnetic helicity. Magnetic helicity evolves according to $\partial_t \langle \mathbf{A} \cdot \mathbf{B} \rangle = \eta \langle \mathbf{B} \cdot \mathbf{J} \rangle$ plus boundary terms. In the absence of flux through boundaries, resistivity limits the formation of a net magnetic helicity to well over a Hubble time (Brandenburg 2001). In a sequence of papers Blackman, Field, and Maron have argued that suppression of early-time mean field growth does not take place (Blackman & Field 2000, 2002; Field & Blackman 2002; Maron & Blackman 2002). They discuss two possibilities for forming a large-scale helical field on the Galactic dynamical time of $\sim 2 \times 10^8$ yr, either by expelling the opposite sign of magnetic helicity from the Galaxy or by exchanging helicity between the forcing supernova and the Galactic scale. Furthermore, Maron & Blackman (2002) show that the helical dynamo could conceivably occur within a Hubble time even for small helical fractions of $\sim 10\%$ and for large Prandtl number. It is clear that this stage is dependent on the disk geometry and physical conditions in the Galaxy and therefore simulations in simplified models may have limitations.

The objective of this paper is to simulate the evolution of the field in stages 1 and 2. We use a simple scalar viscosity and resistivity MHD model of the plasma: this is a simplification of the dissipative processes. For example, a more realistic model for the warm partially ionized interstellar medium would include ambipolar diffusion (Zweibel & Brandenburg 1997), and the fully ionized protogalactic plasmas should have a tensorial viscosity of the Braginskii form (Braginskii 1965; Mal'ushkin & Kulsrud 2002). Such issues will be addressed in future papers. The stirring of the plasma (by supernovae in the Galaxy and turbulence created by collapse in the protogalaxy) is clearly compressible, but the vortical part of the flow is probably well modeled by incompressible motions. For this reason and computational tractability, we use incompressible MHD equations. In stage 1 we find that the field grows exponentially with a $k^{3/2}$ spectrum terminated by the resistive scale, in accord with the Kulsrud-Anderson theory. There are four key results from our stage 2 simulations. First, the energy of the magnetic field grows to a saturated level equal to the kinetic energy of the stirred flow. Second, the magnetic field energy is contained in the small resistive scales. Third, the predominant straining and folding of the field in saturation comes from the stirring-scale motions. Fourth, the field is in the form of long thin folds (stripes) where the variation of \mathbf{B} across itself is much faster than the variation of \mathbf{B} along itself.

2. A HEURISTIC MODEL OF NONLINEAR MAGNETIC FIELD GROWTH

In this section we present a simple model of the magnetic field growth. Numerical evidence for this model is presented in the subsequent sections. We introduce many scales and definitions, and for convenience these are summarized in Table 2.

We take v_λ to be the velocity at scale λ . The flow is forced at scale λ_f with velocity v_f and a timescale $t_f = \lambda_f/v_f$. In the weak-field limit (stage 1) the approximate form of v_λ has been known since the seminal paper by Kolmogorov (1941). Specifically, $v_\lambda \sim v_f (\lambda/\lambda_f)^{1/3}$ in the range $\lambda_\nu < \lambda < \lambda_f$, where λ_ν is the viscous scale to be defined. The eddy turnover time at scale λ , $t_\lambda \sim \lambda/v_\lambda$, increases with scale. At the viscous scale the viscous damping time and the eddy turnover time are comparable ($t_\nu \sim \lambda_\nu^2/\nu \sim \lambda_\nu/v_\nu$). Thus,

$$\lambda_\nu \sim \lambda_f \text{Re}^{-3/4}, \quad (1)$$

where $\text{Re} = (v_f \lambda_f/\nu)$ is the Reynolds number and ν is the coefficient of viscosity. In the interstellar medium of our Galaxy Re is in the range 10^4 – 10^6 . The eddy turnover time at the viscous scale is $t_\nu \sim t_f \text{Re}^{-1/2}$ ($t_\nu \sim 10^5$ yr in our Galaxy), and the viscous-scale velocity is $v_\nu \sim v_f \text{Re}^{-1/4}$.

Our model is based on the assumption that at a given time there is a *single* scale that is amplifying the field most rapidly. Let us call this the shearing scale and denote it λ_s . The velocity at this scale is v_s , and the eddy turnover time (shear timescale) is $t_s = \lambda_s/v_s$. The field is being amplified at a rate $\gamma \sim (1/t_s)$. The magnetic field is destroyed at the resistive scale λ_η where growth is balanced by resistive diffusion, i.e., $t_s \sim \lambda_\eta^2/\eta$, with η the coefficient of resistive diffusion. Thus,

$$\lambda_\eta = (\eta t_s)^{1/2} = \lambda_f (\text{Re}_M)^{-(1/2)} \left(\frac{t_s}{t_f} \right)^{1/2}, \quad (2)$$

where $\text{Re}_M = (v_f \lambda_f/\eta)$ is the magnetic Reynolds number. In the Galaxy $\text{Re}_M \sim 10^{19}$ – 10^{20} and the resistive scale is of order 10^8 – 10^{10} cm. In truth the resistive scale is probably unimportant since above the resistive scale other dissipative and kinetic effects become important (Lithwick & Goldreich 2001). For example, at 10^{11} – 10^{13} cm ambipolar drift of the plasma through the neutrals changes the field dynamics (Zweibel & Brandenburg 1997; Kulsrud & Anderson 1992).

In the kinematic stage (stage 1) the eddies at the viscous scale amplify the field most rapidly and therefore $\lambda_s = \lambda_\nu$ and the growth rate $\gamma \sim 1/t_s \sim 1/t_\nu$. The scale of the field decreases at a similar exponential rate until limited by dissipation (resistance in the computer code). The field at the end of stage 1 is strong enough to affect the stirring eddies, i.e., $B^2/(4\pi) = \frac{1}{2} \rho v_\nu^2$ (which in the Galaxy gives $B \sim 0.1 \mu\text{G}$). The small-scale field is in the form of long folds of length λ_ν and width λ_η (see below; see also Schekochihin et al. 2002c). This field resists bending in a similar way to a smooth field: its response to shearing is somewhat like the wound elastic inside baseballs and golf balls (Appendix C).

Now consider the growth when the magnetic field becomes strong enough to become dynamically important (stage 2). We assume that for $\lambda < \lambda_s$ the velocity is too weak to shear and amplify the field, i.e., $\frac{1}{2} \rho v_\lambda^2 < B^2/(8\pi)$. For $\lambda > \lambda_s$ the velocities are approximately unaffected since $\frac{1}{2} \rho v_\lambda^2 > B^2/(8\pi)$. Therefore, $v_\lambda \sim v_f (\lambda/\lambda_f)^{1/3}$ for $\lambda > \lambda_s$; again the smaller the kinematic velocity scale, the faster the eddy turnover. The shearing scale is then the smallest scale that is still capable of bending the field, i.e., $\frac{1}{2} \rho v_s^2 = B^2/(8\pi)$. Note that we have compared v_λ with the total magnetic field, not just the field at scale λ . The evolution of the field is therefore given by

$$\frac{1}{8\pi} \frac{dB^2}{dt} \sim \frac{v_s}{\lambda_s} \frac{B^2}{8\pi} \sim \frac{1}{2} \rho \frac{v_s^3}{\lambda_s} \sim \epsilon. \quad (3)$$

TABLE 2
SCALES AND DEFINITIONS

Parameter	Definition	Parameter	Definition
v_λ	Velocity at scale λ	B_λ	Magnetic field at scale λ
ν	Kinematic diffusivity	η	Resistive diffusivity
λ_ν	Viscous scale	λ_η	Resistive scale
λ_f	Forcing scale (=1)	v_f	Outer scale rms velocity (=1)
λ_s	Shear scale	v_s	Shear-scale velocity
$\text{Re} = v_f \lambda_f / \nu$	Reynolds number	$\text{Pr} = \nu / \eta$	Prandtl number
$\lambda_a = 3/N$	Aliasing (resolution) scale	N^3	Grid size
$t_f \sim \lambda_f / v_f$	Forcing timescale	$t_s \sim \lambda_s / v_s$	Shear timescale
λ_\perp	Transverse folding scale	λ_\parallel	Longitudinal folding scale
$f = \lambda_\parallel / \lambda_\perp$	Field-line folding factor	$s = k/2\pi = 1/\lambda$	Wavenumber

Note that ϵ is the constant energy flux of the Kolmogorov cascade. Equation (3) states that at scale λ_s , a significant fraction of the cascading energy is converted into magnetic energy. These heuristic scalings do not, of course, determine the exact fraction of cascade energy that gets converted into magnetic energy. Solving equation (3) with $B^2/(8\pi) = \frac{1}{2}\rho v_\nu^2$ at $t = 0$ gives

$$\frac{B^2}{8\pi} = \frac{1}{2}\rho v_\nu^2 + \epsilon t \quad (4)$$

and $(t_s/t_f) = B^2/(4\pi\rho v_f^2)$. As expected, the shearing time and scale increase during stage 2. When $t \sim t_f \sim (\lambda_f/v_f)$, one large-scale stirring time, the shear scale has reached the forcing scale and $B^2/(8\pi) \sim \frac{1}{2}\rho v_f^2$. At this point the growth ceases as shearing at all scales is suppressed by the field. This does not mean that all motion is suppressed: one expects Alfvén oscillations that exchange energy between the tangled field and motion (Appendix C).

In our discussions so far we have ignored the structure of the magnetic field; this obviously needs justification. As we have already remarked, during the kinematic stage the field grows at all scales but the field energy becomes peaked at the small scales. In the course of amplification and entanglement, the field develops structure not identifiable in the power spectrum. The structure of this field has been shown (Schekochihin et al. 2002c) to be folded into a reduced-tension state. We characterize this structure by the quantities

$$k_\perp^2 = \frac{\langle (\mathbf{B} \times \nabla \times \mathbf{B})^2 \rangle}{\langle B^4 \rangle}, \quad k_\parallel^2 = \frac{\langle (\mathbf{B} \cdot \nabla \mathbf{B})^2 \rangle}{\langle B^4 \rangle}, \quad (5)$$

$$k_p^2 = \frac{\langle (\nabla B^2/2)^2 \rangle}{\langle B^4 \rangle}, \quad k_o^2 = \frac{\langle (\mathbf{B} \cdot \nabla \times \mathbf{B})^2 \rangle}{\langle B^4 \rangle}, \quad (6)$$

and a scale measure of the spectrum,

$$k_b^2 = \frac{\int k^2 E_b(k) dk}{\int E_b(k) dk}. \quad (7)$$

The corresponding lengths are defined in the obvious way, i.e., $\lambda_\parallel = 2\pi/k_\parallel$ and $\lambda_\perp = 2\pi/k_\perp$. We also define a field-line folding factor $f = k_\perp/k_\parallel$, which parameterizes the magnetic tension per energy and the unwinding time of field lines; typically f is large. We normalize with $\langle B^4 \rangle$ instead of $\langle B^2 \rangle^2$ because it has similar statistics as the squared magnetic force

terms. In the simulations, $k_\perp/k_b \sim 0.58$ with fluctuations of 3%, whereas the kurtosis $(\langle B^4 \rangle / \langle B^2 \rangle^2)$ varies by 200% (Schekochihin et al. 2002d). Therefore, either k_\perp or k_b may be used to define the magnetic scale. In this paper we do not use k_o further except to point out that it typically lies in the range $k_\perp > k_o > k_\parallel$.

At the end of stage 1, $k_\perp \sim k_p \sim \mathcal{O}(k_b) \sim \mathcal{O}(1/\lambda_\eta)$ but $k_\parallel \sim \mathcal{O}(1/\lambda_\nu) \ll k_\perp$. Let \mathbf{b} be the unit vector in the direction of \mathbf{B} . The folded field has relatively straight sections with $\mathbf{b} \cdot \nabla \mathbf{b} \sim \mathcal{O}(1/\lambda_\nu)$ and highly curved corners where $\mathbf{b} \cdot \nabla \mathbf{b} \sim \mathcal{O}(1/\lambda_\eta)$ (Schekochihin et al. 2002c). The strength of the field in the corners is reduced so that the tension force $(\mathbf{B} \cdot \nabla \mathbf{B})$ is $\mathcal{O}(\langle B^2 \rangle / \lambda_\nu)$ or less in the corners and straight sections. The distance between corners is probably $\mathcal{O}(\lambda_\nu)$, although we do not know this for sure.

During nonlinear growth (stage 2) the shearing eddies presumably act on the magnetic field in a manner similar to the viscous eddies in the kinematic (stage 1) growth. As we shall discover below, unfolding flows produced by the magnetic tension can change parts of the spectrum. However, at high Prandtl numbers most of the magnetic energy remains in folds deep in the viscous region where unfolding is highly damped. Thus, such flows can be ignored in obtaining the basic behavior at high Prandtl number. We therefore discuss first the evolution of the structure, assuming that at every stage the field is stretched only by the shearing-scale eddies, and then estimates of the unfolding flows are given.

In a recent paper (Schekochihin et al. 2002b) we have constructed a self-similar model of the nonlinear growth. We argue that during this phase $\lambda_\parallel \sim \lambda_s$. During the nonlinear growth the folds get thinner and flux is destroyed at the resistive scale. Thus, we expect $\lambda_\perp \sim \lambda_\eta = (\eta t_s)^{1/2}$. Note that the resistive scale increases with time. The resistive destruction of flux will affect the growth of the field in equation (3). The effect of resistivity is to decrease the growth rate of B^2 by a factor of $\frac{3}{8}$ in short correlation time models of stage 1. We expect therefore that a similar numerical factor should appear in equation (3) and that a finite part of the cascade energy goes to resistive heating.

After the field strength has reached saturation, i.e., when $B^2 \sim \frac{1}{2}\rho v_f^2$ and $\lambda_s = \lambda_f$, the structure of the field continues to evolve somewhat. Resistive weakening of the field will allow further stretching by the large-scale eddies. The resistive weakening and the large-scale stretching both occur at the forcing timescale, i.e., $t_f \sim t_\eta \sim t_s$. The length of the folds increases until $\lambda_\parallel \sim \lambda_f$. Smaller scale eddies remain too weak to do any further stretching. One also expects folds with $\lambda_\parallel \sim \lambda_f$ to be made during this phase. Thus, the folded

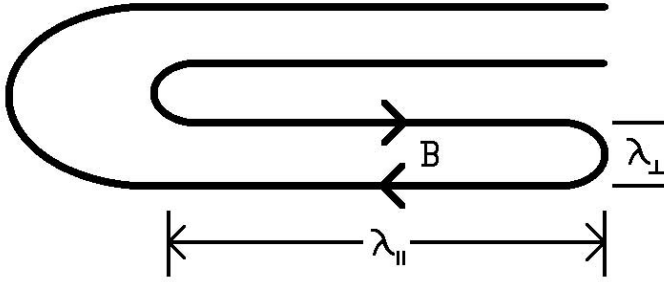


FIG. 1.—Schematic of longitudinal (L_{\parallel}) and transverse (L_{\perp}) folding scales of the magnetic field. Magnetic fields tend to be straight where they are strong and curved where they are weak, thus reducing their rms tension. One also sees how magnetic field lines are strained and folded. An initially straight magnetic field is folded twice here to produce the configuration shown.

structure is continuously regenerated. Eventually the field structure reaches steady state with the folds being destroyed by resistivity at the small scales and refolded at the large scales. *The saturated state has a single straining scale and timescale: the forcing scale.* We have not been able to deduce the shape of the magnetic spectrum from heuristic arguments. From simulations we find that the magnetic energy is dominated by the subviscous scales.

The above discussion is based on the assumption of a *single* stretching scale and that the eddies at that scale amplify the field in a manner similar to the viscous eddies in the kinematic growth: stage 1. We are therefore explicitly ignoring any flows correlated with magnetic field structure. However, the magnetic tension forces in stage 2 drive such flows, and they can change the structure of the field. Specifically, during growth, tension forces unfold and straighten the field over a range of perpendicular scales. This follows from balancing the tension forces with viscous or inertial forces. Consider a particular fold (not necessarily a typical fold) of length L_{\parallel} and perpendicular scale L_{\perp} (see Fig. 1). The magnetic tension is of order B^2/L_{\parallel} in the fold. Balancing tension with inertial forces yields an unfolding velocity,

$$v_i \sim V_A \sim v_s, \quad (8)$$

where $V_A = (B^2/4\pi\rho)^{1/2}$ is the Alfvén velocity and $V_A \sim v_s$ follows from the nature of the back-reaction. Thus, the inviscid unfolding rate, v_i/L_{\parallel} , of folds with $L_{\parallel} < \lambda_s$ is faster than the shearing rate v_s/λ_s . Balancing tension and viscosity yield a viscous unfolding velocity,

$$v_u \sim \frac{V_A^2}{\nu} \left(\frac{L_{\perp}^2}{L_{\parallel}} \right). \quad (9)$$

The unfolding is viscous when v_u is less than v_i , or equivalently $L_{\perp} < \lambda_{\nu}^{2/3} \lambda_s^{-1/6} L_{\parallel}^{1/2}$. The viscous unfolding rate v_u/L_{\parallel} is faster than the shearing rate for folds with $L_{\perp} > \lambda_{\nu}^{2/3} \lambda_s^{-2/3} L_{\parallel}$. During the stage 2 growth phase, we have $L_{\parallel} \sim \lambda_{\parallel} \sim \lambda_s$ (Schekochihin et al. 2002b). Thus, from equation (9) we find that folds with $\lambda_{\nu}^{2/3} \lambda_s^{1/3} > L_{\perp} > \lambda_{\eta}$ remain folded during growth. Folds with $\lambda_s > L_{\perp} > \lambda_{\nu}^{2/3} \lambda_s^{1/3}$ unfold inviscidly (Alfvénically) at roughly the folding rate; thus, we expect some folding in this range.

At saturation of the field strength $B^2/(8\pi) = \frac{1}{2}\rho v^2$ the folds have elongated until $L_{\parallel} = \lambda_{\parallel} = \lambda_f$. In this final saturated state the folded range is $\text{Re}^{1/4} \text{Pr}^{-1/2} < L_{\perp}/\lambda_{\nu} < \text{Re}^{1/4}$. At scales above the folded range the unfolding and stretching timescales

are equal. Fields on these scales are in a dynamic state of folding and unfolding. At Prandtl number of order 1 the folded range disappears and the unfolding rate is comparable to the shearing rate at all scales. In simulations with $\text{Pr} \sim 1$ we observe that $\lambda_{\perp} < \lambda_{\parallel} < \lambda_f$ and the field and spectrum visually appear to resemble the $\text{Pr} \gg 1$ case; we do not understand this. Although the computational evidence indicates that the stirring-scale velocities produce all the folding in saturation, velocity fluctuations persist below the forcing scale down to the viscous scale, λ_{ν} (see § 5.2). These fluctuations do not appear to affect any net folding.

The discussion of folding above is, unfortunately, not very precise. The basic scenario is seen in the simulations, but the detailed scalings are not obtainable with the available resolution. For example, we observe that at high magnetic Prandtl number the saturated field is predominantly in the form of viscously dominated folds with length λ_f and perpendicular scale λ_{η} . We also observe a single straining scale in saturation, namely, the forcing scale.

3. EQUATIONS AND DEFINITIONS

We normalize the magnetic field so that $\mathbf{B}/(4\pi\rho)^{1/2} \rightarrow \mathbf{B}$; i.e., \mathbf{B} has units of velocity. The equations we simulate are then

$$\partial_t \mathbf{v} = -\mathbf{v} \cdot \nabla \mathbf{v} - \nabla \left(\mathbf{P} + \frac{\mathbf{B}^2}{2} \right) - \nabla \cdot \Pi + \mathbf{B} \cdot \nabla \mathbf{B} + \nu \nabla^2 \mathbf{v} + \mathbf{F}, \quad (10)$$

$$\partial_t \mathbf{B} = \nabla \times (\mathbf{v} \times \mathbf{B}) + \eta \nabla^2 \mathbf{B}, \quad (11)$$

$$\nabla \cdot \mathbf{v} = 0, \quad \nabla \cdot \mathbf{B} = 0. \quad (12)$$

These equations of incompressible MHD are solved using a pseudospectral code in a unit cubic box with periodic boundaries. We withhold details about the computer code not necessary for understanding the results (see Maron & Goldreich 2001; Maron 2000). A 256^3 grid with spatial dimension l^3 has Fourier wavenumbers $s = k/(2\pi)$ extending from -85 to $+85$, where we have employed the $\frac{2}{3}$ rule to avoid aliasing errors. We find (see Appendix B) that without sufficient resistivity (η) the important magnetic field structure is destroyed by the dealiasing truncation. The simulations are forced by adding random velocity increments at the large scales ($s = 1 - 2$) every time step, effectively white-noise forcing that maintains a constant time-averaged energy input. The magnetic field has no mean component, and the forcing has no preferred kinetic helicity.

The object of this work is to study the dynamics when the magnetic field is strong enough to react back on the turbulence. It is clear from the introduction that to be in the relevant regime we require $\lambda_{\eta} \ll \lambda_{\nu} \ll \lambda_f$. We arrange the forcing scale to be at the largest computational scale ($\lambda_f \sim 1$). To get large Prandtl numbers, we set the resistive scale to be at the smallest computational scale ($\lambda_{\eta} \sim 3\lambda_f/N$), where N is the number of grid elements on each cube edge. During the kinematic growth, this requires $\eta \sim 9\lambda_f^{3/2} v_f^{3/2} \nu^{-1/2} N^{-2}$. For our studies it is desirable to have λ_{ν} small enough so that a true kinematic inertial range exists; this requires $\lambda_{\nu} \geq \lambda_f/8$. In the heuristic model of § 2 we show that once the magnetic field is strong enough to react back on the velocity, the resistive scale increases. Thus, we expect that if the resistive scale is resolved in the linear regime, it will remain resolved in the nonlinear regime.

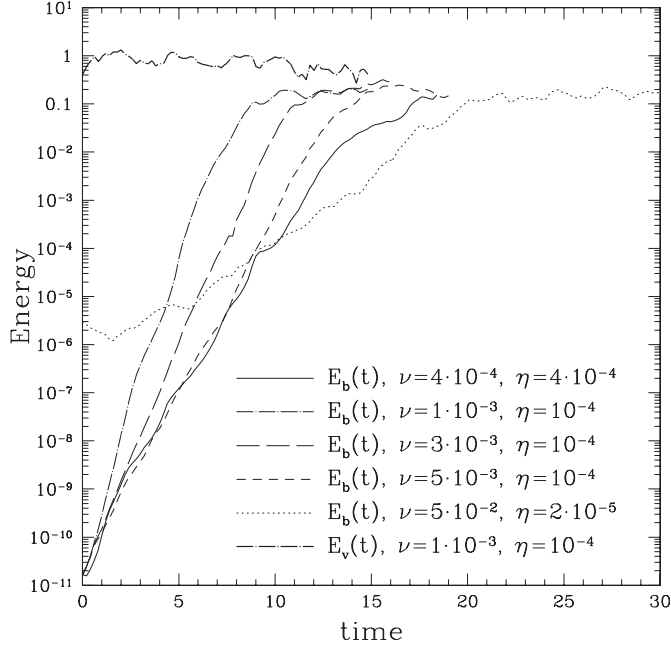


FIG. 2.—Exponential magnetic energy growth for a sequence of viscosities, and $E_v(t)$ for simulation A4. Parameters for the simulations (A1–A5) are given in Table 4.

The available spectral resolution with our computational resources is a 256^3 spectral grid or coarser. Thus, we can achieve a range of scales of order 50. Unfortunately, we find that to obtain the well-known kinematic spectrum of stage 1 (Kulsrud & Anderson 1992; Schekochihin et al. 2002a) a Prandtl number of at least 2500 is required. Such a Prandtl number is only possible when the largest scale is the viscous scale ($\lambda_f \sim \lambda_\nu$). We have, nonetheless, studied the role of viscosity and the inertial range in a sequence of simulations with λ_ν ranging between λ_f and λ_η . Clearly, larger simulations, $N > 256$, would be desirable to obtain large Re and Pr simultaneously.

We define the one-dimensional kinetic and magnetic energy spectra as $E_v = \int E_v(s) ds$ and $E_b = \int E_b(s) ds$. The heuristic definitions of scales and times in § 2 are replaced with more precise definitions that are calculated in the simulations. Thus, we define timescales for resistivity (t_η), vorticity (t_w), and shear (t_s) by

$$t_\eta = \frac{1}{k_\perp^2 \eta}, \quad t_w = 2\pi \langle (\nabla \times \mathbf{v})^2 \rangle^{-1/2},$$

$$t_s = \frac{\langle B^2 \rangle}{\epsilon}, \quad (13)$$

where ϵ is the energy input rate (with our forcing $\epsilon = 1$); t_s is indirectly linked to the shear time through $t_s \sim B^2/\epsilon \sim v_s^2/\epsilon \sim \lambda_s/v_s$, where λ_s and v_s correspond to the scale and velocity of the dominant shear. We also define the viscous scale λ_ν to correspond to the peak of the function $k^3 E_v(k)$.

The parameters for each simulation are given in Table 4 in Appendix A.

4. MAGNETIC FIELD GROWTH

In this section we present simulations of the growth of field from weak initial values. Growth occurs in two stages: linear and nonlinear. We found that for all simulations with $\text{Pr} \gg 1$

the field grew to rough equipartition $B^2 \sim v_f^2$ and remained at this level in a saturated equilibrium state. We discuss the saturated state in § 5. In § 4.2 we include (for completeness) a discussion of the $\text{Pr} < 1$ simulations of growth.

4.1. Growth of a Weak Magnetic Field, $\text{Pr} > 1$

The magnetic field is initially weak during the linear stage, and the kinetic spectrum has the Kolmogorov form. Magnetic fields grow exponentially at the rate of the turbulent shear. Since the viscous-scale eddies shear the fastest, magnetic growth proceeds at the viscous timescale t_ν . Kulsrud & Anderson (1992; see also Kazantsev 1968; Gruzinov, Cowley, & Sudan 1996; Schekochihin et al. 2002a) found that at high Pr a dynamically weak magnetic field grows exponentially with a $k^{3/2}$ subviscous-scale spectrum terminating at the resistive scale.

We ran simulations starting from a weak magnetic field for a sequence of five viscosities, all with $\text{Pr} \geq 1$. For each value of the viscosity, the resistivity is assigned the smallest value such that most of the magnetic energy is destroyed by resistivity before reaching the dealiasing scale. The ID numbers of these five simulations are A1–A5 (see Table 4 in Appendix A), and their energy and spectral evolutions are shown in Figures 2–5. Magnetic energies grow exponentially in all cases until the nonlinear stage is reached. The growth times t_g are given in Table 3, expressed in the form $E_b(t) \sim e^{t/t_g}$. The $k^{3/2}$ exponent is seen only when $\text{Pr} \geq 2500$, as with simulation A1, where sufficient range exists between the viscous and resistive scales (Fig. 4). The $k^{3/2}$ spectrum is especially robust in the simulation with zero resistivity (simulation A0; Fig. 5). However, this simulation is not without concern for its physical validity since the dealiasing destroys important features of the magnetic structure not apparent in the spectrum. (This is addressed further in §§ 5.3 and 5.1 and Appendix B.) We see that very roughly $t_g \propto t_w$ for simulations A1–A4. Simulation A5 does not fit this rough scaling since

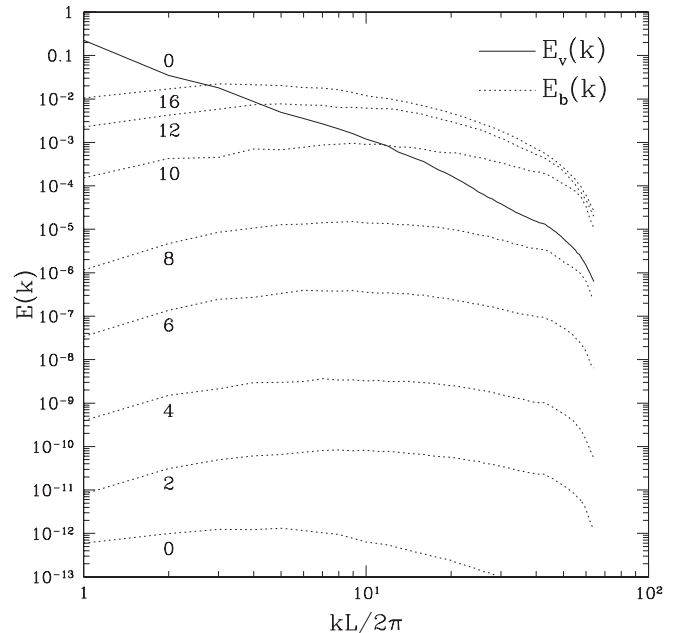


FIG. 3.—Evolution of the magnetic spectrum for simulation A3, with numbers indicating times. The spectrum at the latest time is in the saturated state.

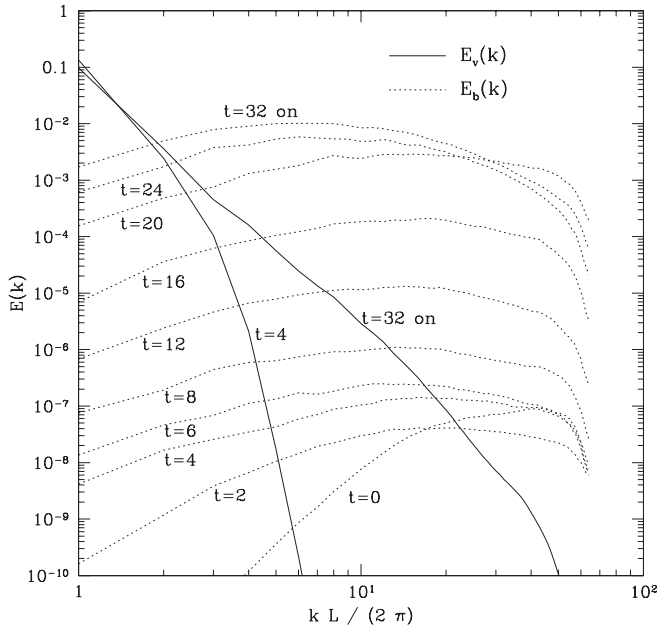


FIG. 4.—Kinetic and magnetic energy spectra for simulation A1, $Pr = 2500$, with $\nu = 5 \times 10^{-2}$ and $\eta = 2 \times 10^{-3}$. The Prandtl number is just large enough to see the linear-stage $k^{3/2}$ magnetic spectrum. Detailed comparison with the kinematic theory was possible in the two-dimensional simulations of Kinney et al. (2000). The lack of a more detailed comparison in three dimensions is simply a consequence of the limited resolution.

it has $Pr = 1$, and therefore the simple kinematic theory described for stage 1 is not valid.

The magnetic kurtosis, $\langle b^4 \rangle / \langle b^2 \rangle^2$, is observed to rise from ~ 3 to ~ 15 during the linear regime and then to return to ~ 3 in the saturated state. These results are expanded on in Schekochihin et al. (2002d).

Since we cannot achieve $Pr \gg 1$ and $Re \gg 1$ simultaneously, we have little evidence for the nonlinear stage of growth described in § 2. The best evidence comes from examining the resistive scale of the magnetic field, which is determined by a balance between shear growth and resistive decay: $t_s \sim \lambda_\eta^2 / \eta$. We note that $\lambda_\eta = \lambda_\perp$ (eq. [5]). From the beginning to the end of the nonlinear stage, λ_\perp is predicted (§ 2) to increase by a factor of $(\lambda_f / \lambda_\nu)^{1/3} \propto \nu^{-1/4}$. The data in Table 3 support this scaling, although the comparison is inexact because the forcing velocity and hence the shear time change slightly from the linear to the saturated state.

4.2. $Pr < 1$

Although the main thrust of this paper is to examine the $Pr \gg 1$ limit (because of its astrophysical relevance), we have for completeness performed three $Pr < 1$ simulations. For $Pr < 1$, subresistive velocities hinder magnetic growth. We establish this with two simulations having the same λ_η and different λ_ν (Figs. 6 and 7). The first (S1) has $\lambda_\nu = \lambda_\eta$, and the second (S2) has $Pr = 0.4$, which from Kolmogorov's inertial range scaling gives $\lambda_\nu \sim 0.5\lambda_\eta$. The only apparent difference between the velocities in these simulations is that S2 has subresistive scale velocity fluctuations. The resolution of S2 is, we believe, sufficient to capture the dynamics. The magnetic energy in simulation S1 grows more quickly than that for simulation S2. We do not know if the subresistive velocities provide a kind of turbulent resistivity (Parker 1979).

In Figures 8 and 9 the magnetic field decays for two simulations with Prandtl number 0.2 and 0.1 (simulations S3 and

S4, respectively). The magnetic Reynolds number for S4 is 250, which is large enough to sustain the magnetic field were the Prandtl number to be greater than 1. Clearly, there is a critical Prandtl number for kinematic growth. However, it is not clear from our simulations how the critical Prandtl number for growth depends on Reynolds number.

5. MAGNETIC SATURATION

All our $Pr \gg 1$ simulations eventually reach a steady state: magnetic saturation. This is the long-term state of MHD turbulence in the absence of a mean magnetic field and with zero mean kinetic helicity. This is the magnetic analog to the Kolmogorov problem for hydrodynamic turbulence. In the saturated state, the magnetic field is strong enough to affect the turbulence at all scales; specifically, $\langle b^2 \rangle = E_b \sim \langle v_f^2 \rangle = E_v$. Note that in two dimensions (Zel'dovich 1957; Kinney et al. 2000) the magnetic field asymptotes to zero and there is no magnetic steady state.

Four consequences of the heuristic model (§ 2) are apparent in the simulations. First, we see from Table 3 that E_b is smaller but of order E_v : notice that they become essentially equal as the Prandtl number increases. Second, the magnetic energy is located at the small, resistive scale $\lambda_\eta = (t_f \eta)^{1/2}$ (see § 5.1). Third, the field is stretched and folded by stirring-scale motions and the magnetic spectrum is largely independent of viscosity. Fourth, the magnetic field is folded into a reduced-tension state (similar to the magnetic structure in the growth phases) where field-line curvature anticorrelates with intensity. We explore evidence for the third and fourth consequences in §§ 5.2 and 5.3, respectively.

5.1. Dissipative Power and Magnetic Scale

Energy injected into the motions at the stirring scale is dissipated via two routes. In the first, energy is transferred from the stirring-scale motions via stretching to the magnetic field at all scales and dissipated by resistivity at the resistive scale. In the second, kinetic energy is cascaded to small scales

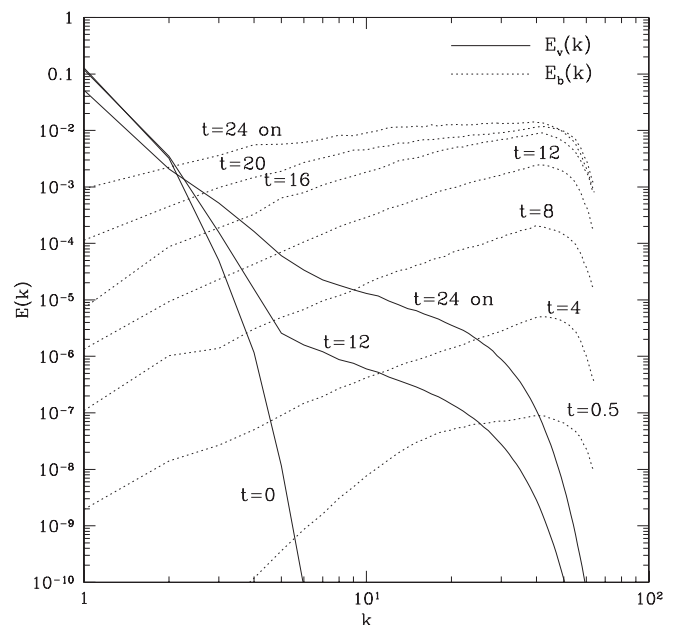


FIG. 5.—Kinetic and magnetic energy spectra for simulation A0, with $\nu = 5 \times 10^{-2}$ and $\eta = 0$. The Prandtl number is undefined; however, for this resolution and viscosity, any value of Pr above 10^4 is functionally equivalent.

TABLE 3
ENERGIES AND TIMESCALES

SIMULATION	ν	η	E_v		E_b SAT	t_g LINEAR	t_w		t_η		s_\perp	
			Linear	Sat			Linear	Sat	Linear	Sat	Linear	Sat
A1.....	5×10^{-2}	2×10^{-5}	0.2	0.16	0.17	1.41	1.5	1.55	4.38	8.8	17.0	12.0
A2.....	5×10^{-3}	1×10^{-4}	0.75	0.38	0.32	0.59	0.45	0.62	1.50	3.5	13.0	8.5
A3.....	3×10^{-3}	1×10^{-4}	0.8	0.40	0.32	0.46	0.35	0.47	1.26	3.5	14.2	8.5
A4.....	1×10^{-3}	1×10^{-4}	0.9	0.60	0.22	0.36	0.25	0.30	0.78	3.1	18.0	9.0
A5.....	4×10^{-4}	4×10^{-4}	1.5	0.60	0.16	0.65	0.12	0.23	0.30	1.8	14.6	6.0
B1.....	5×10^{-2}	1×10^{-5}	...	0.16	0.17	2.0	...	12.9	...	14.0
B2.....	5×10^{-3}	4×10^{-5}	...	0.3	0.4	0.69	...	4.4	...	12.0
B3.....	3×10^{-3}	4×10^{-5}	...	0.3	0.3	0.57	...	4.4	...	12.0
B4.....	1×10^{-3}	4×10^{-5}	...	0.5	0.3	0.31	...	3.5	...	13.4
B5.....	4×10^{-4}	1×10^{-4}	...	0.55	0.3	0.20	...	3.4	...	8.6
B6.....	1×10^{-4}	1×10^{-4}	...	0.55	0.3	0.11	...	3.1	...	9.0

NOTES.—“Linear” and “sat” denote the linear and saturated states, averaged over a suitable length of time. E_v and E_b are the kinetic and magnetic energies, t_g is the exponential magnetic growth time during the linear phase, t_w is the vorticity time, t_η is the resistive time, and $s_\perp = k_\perp / (2\pi)$ is the magnetic wavenumber. The 256^3 simulations were run for 5 crossing times (λ_f / v_f).

where it is dissipated by viscosity. We find that the energy dissipated by each mechanism is about equal in our solutions. To compare the spectral distribution of energy and dissipation for the saturated state, we plot the logarithm of each quantity. For the kinetic and magnetic spectra, we plot $\ln(10)kE(k)$, and for the viscous and resistive power, we plot $2\nu \ln(10)k^3 E_v(k)$ and $2\eta \ln(10)k^3 E_b(k)$, respectively.

In Figures 10 and 11 we compare two simulations: A4, a 128^3 simulation with $\nu = 10^{-3}$ and $\eta = 10^{-4}$, and B4, a 256^3 simulation with $\nu = 10^{-3}$ and $\eta = 4 \times 10^{-5}$. It is clear that the magnetic energy is contained in a scale that decreases with η . This is supported by the observation that the peak of the magnetic spectrum (*solid line*) occurs where the resistive dissipation becomes large. Viscous dissipation remains at a medium scale as expected from hydrodynamics. Both of these simulations are barely resolved as can be seen from the structure at the resolution (aliasing) cutoff. The issue of adequate resolution is discussed further in Appendix B.

5.2. Shear Timescale

In § 2 we have presented a scenario for nonlinear suppression of growth by the magnetic field. In this scenario the field suppresses the net shearing by those eddies with kinetic energy density less than the magnetic field energy density. Thus, in the saturated state only the forcing-scale eddies are sufficiently energetic to continue to stretch and fold the field. Nevertheless, in saturation (with $\nu \leq 3 \times 10^{-3}$) the kinetic spectrum decreases less rapidly than k^{-3} (Figs. 12 and 13), suggesting that small-scale shear dominates. Also note that the vorticity time, t_w , does not change significantly between the linear and saturated states (see Table 3) as might be expected if the shearing of the small scales is suppressed. However, the magnetic spectrum is largely unaffected by the presence of these small-scale velocities (see Figs. 12 and 13). Indeed the magnetic spectrum is remarkably insensitive to changes in viscosity at fixed resistivity. We tentatively interpret these

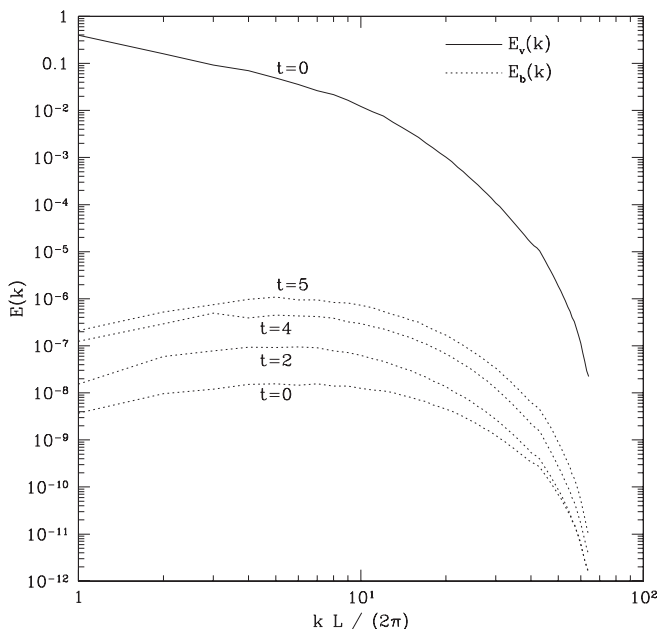


FIG. 6.—Simulation S1, with $\nu = 10^{-3}$, $\eta = 10^{-3}$, and $Pr = 1$. The magnetic field grows robustly.

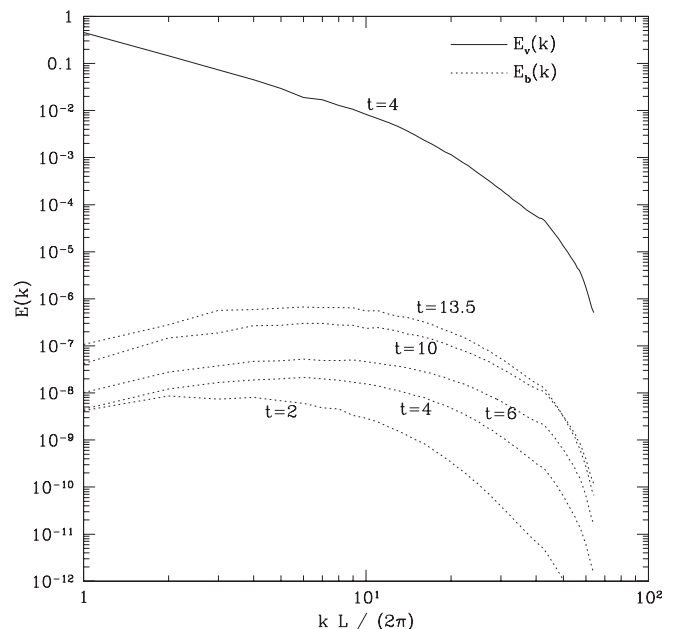


FIG. 7.—Simulation S2, with $\nu = 4 \times 10^{-4}$, $\eta = 10^{-3}$, and $Pr = 0.4$. Unlike in Fig. 6, the magnetic field grows slowly.

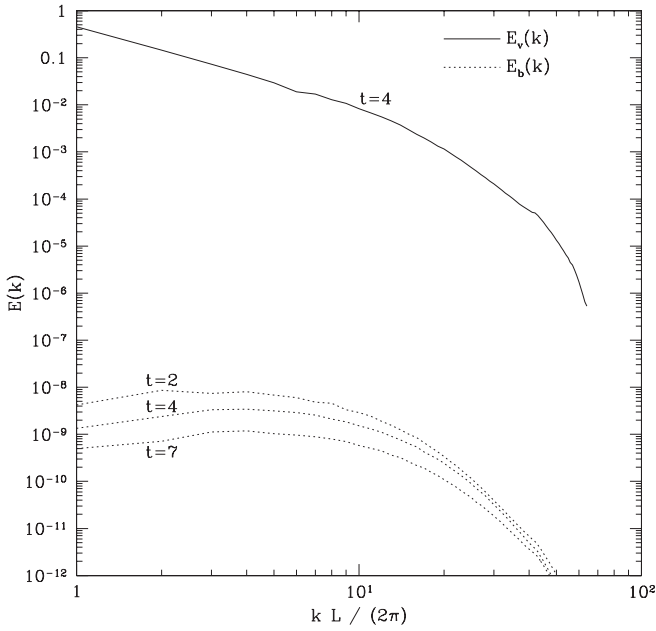


FIG. 8.—Simulation S3, with $\nu = 4 \times 10^{-4}$, $\eta = 2 \times 10^{-3}$, and $\text{Pr} = 0.2$. The magnetic field decays.

observations as showing that the stirring-scale motions stretch and fold the field and that the small-scale motions are oscillatory motions (perhaps Alfvén waves) that cyclically exchange energy between \mathbf{v} and \mathbf{B} (Appendix C). Further work is needed to establish the validity of this interpretation.

Further evidence for the hypothesis that the stirring scale is the single stretching and folding scale comes from examining the resistive scale and time. As we explained in § 2, the resistive scale, λ_η , and resistive time, t_η , increase from the linear phase to the saturated phase. The data of Table 3 support the prediction that λ_η increases by a factor proportional to $\nu^{-1/4}$. Furthermore, the resistive time is insensitive to

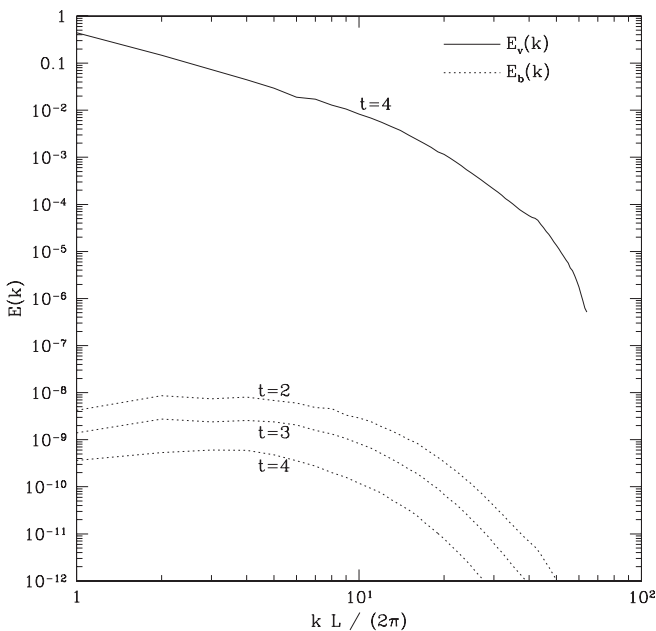


FIG. 9.—Simulation S4, with $\nu = 4 \times 10^{-4}$, $\eta = 4 \times 10^{-3}$, and $\text{Pr} = 0.1$. The magnetic field decays.

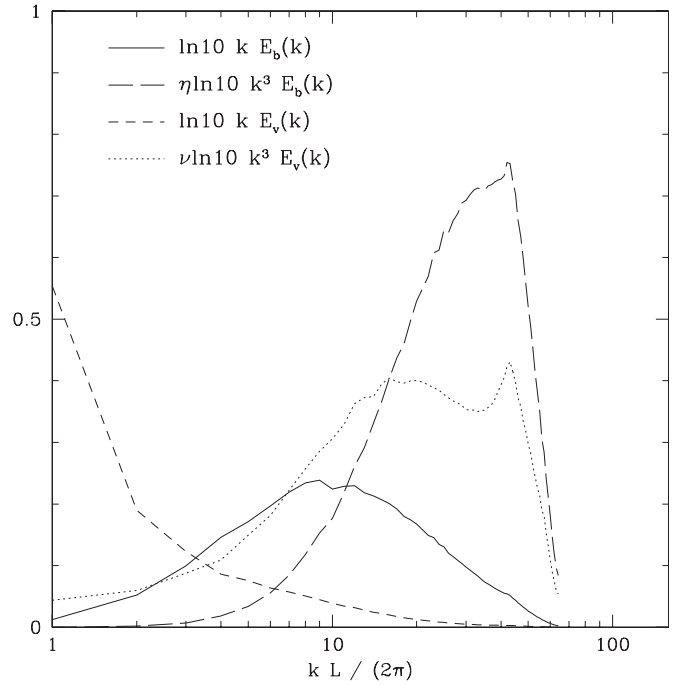


FIG. 10.—Energy and dissipation spectra for the velocity and magnetic fields from simulation A4, which has $\nu = 10^{-3}$ and $\eta = 10^{-4}$.

the viscosity (at fixed resistivity) and therefore the presence of small-scale motions. The t_η is not expected to be exactly independent of viscosity in the saturated state because the larger viscosities influence the forcing-scale velocities and hence the stirring-scale shear rate. For example, for case A1, the viscous damping rate νk_f^2 is within a factor of 1.5–3 of the approximate eddy turnover rate $(2E_v)^{1/2} k_f$ at the forcing scales $2\pi \leq k_f \leq 4\pi$.

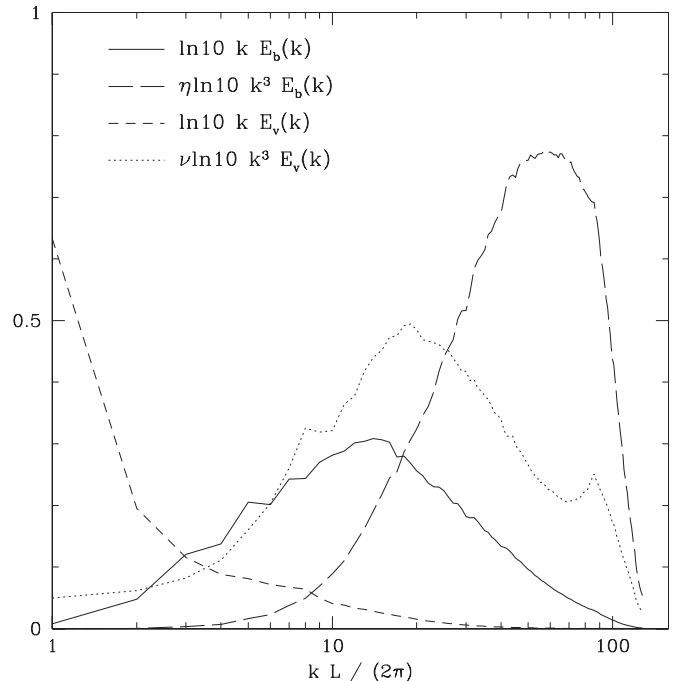


FIG. 11.—Energy and dissipation spectra for the velocity and magnetic fields from simulation B4, which has $\nu = 10^{-3}$ and $\eta = 4 \times 10^{-5}$. The magnetic spectrum of simulation B4 peaks at a larger k than for simulation A4.

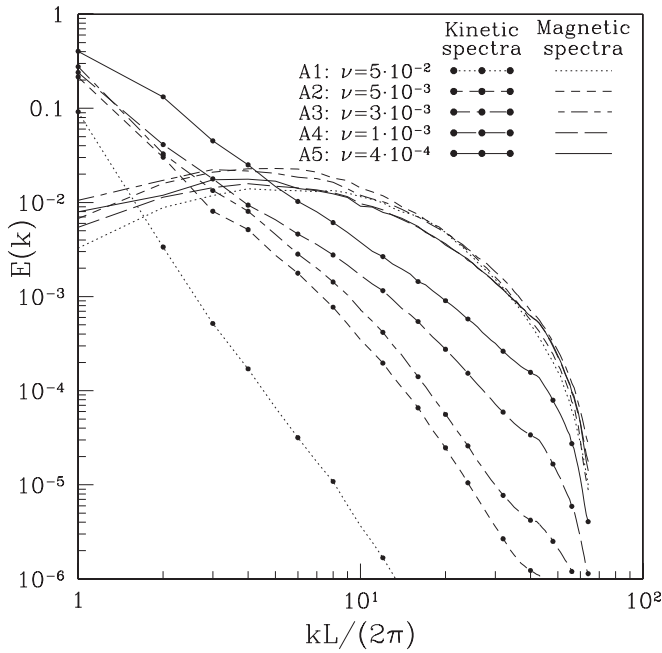


FIG. 12.—Saturated spectra for the 128^3 simulations A1–A5 (Table 4), representing a sequence of viscosities at (approximately) fixed resistivity. Each spectrum represents an average over five forcing timescales. The magnetic spectrum is largely independent of viscosity.

5.3. Magnetic Structure

The magnetic field has a characteristic (folded) structure in the saturated state. The folding in saturation is similar to that in the linear growth phase (Schekochihin et al. 2002d). We quantify this structure by measuring the longitudinal and transverse magnetic scales, λ_{\parallel} and λ_{\perp} (see eqs. [5] and [6]). In Figure 14 we plot λ_{\parallel} and λ_{\perp} of the saturated states for a range ν and η . The data in Figure 14 are consistent with $\lambda_{\perp} \sim \lambda_{\eta} \sim \eta^{1/2}$, which would be expected if the shear timescale is constant and shear balances resistivity. The λ_{\parallel} is approximately constant (in the resolved range) and equal to the outer scale of unity.

Folded structure reduces the magnetic tension forces that drive unwinding of the small-scale magnetic field. In a recent paper (Schekochihin et al. 2002d) we demonstrated that in the saturated state the curvature of the field lines is anticorrelated with the field strength. The corners of the folds have large curvature but small field strength. Therefore, less generation of small-scale velocities by the unwinding of small-scale magnetic fields occurs. The reduction is apparently large enough that magnetic energy “cascades” from the forcing scale to the resistive scale without substantial loss to unwinding. This phenomenon is reflected in the near independence of the magnetic spectrum on viscosity (Figs. 12 and 13), and it is observed directly in the tension release simulations of § 5.5. The kinetic spectra also have greatly reduced magnitudes compared to the magnetic spectra at high k . The magnetic spectrum will be unaffected by unwinding if the forcing-scale shear, which creates the field, is faster than the unwinding, which removes it. The scalings of § 2 suggest that this is the case if $\lambda_{\parallel} \sim \lambda_f$. This condition is shown to be approximately satisfied in Figure 14.

During the linear phase, the intermittency of the magnetic field grows (Schekochihin et al. 2002a). The field is less intermittent in the saturated phase: in simulations the magnetic kurtosis, $\langle b^4 \rangle / \langle b^2 \rangle^2$, rises from ~ 3 to ~ 15 during the linear

regime and then returns to ~ 3 in the saturated state. The reduction in intermittency probably arises because spatial regions with weak field continue to amplify after regions with strong field have saturated until the whole field reaches a state of closely packed, comparably strong magnetic folds. This issue will be addressed further in future publications.

5.4. Large Initial Magnetic Field

As we have discussed, at high Prandtl number the kinematic theory (Kulsrud & Anderson 1992; Kazantsev 1968; Gruzinov, Cowley, & Sudan 1996; Schekochihin et al. 2002a) predicts that an initially weak field grows exponentially with a $k^{3/2}$ spectrum, which simulation confirms. The $k^{3/2}$ spectrum is after a transient period (of order the viscous eddy turnover time) independent of the initial spectral shape. The magnetic energy is therefore dominated by small-scale structure at the beginning of the nonlinear phase, and simulations show that it remains so through subsequent evolution to the saturated state. In this section we examine the evolution when the magnetic field is initially strong and organized at low k . The strong magnetic tension would, at least initially, inhibit the formation of small-scale fields. Nevertheless, we find that the magnetic structure evolves to the same small-scale saturated state that resulted from the weak initial field simulation. In general, we have observed no magnetic hysteresis.

Simulation L3 has an initial magnetic energy of unity, which is confined to modes with $k/2\pi \leq 4$. The viscosity is 3×10^{-3} and the resistivity is 10^{-4} , both of which are identical to simulation A3. The viscous scale is smaller than the initial magnetic scale. Subsequent evolution restores the magnetic spectrum to the saturated state of simulation A3, as shown in Figure 15. Simulation L4 has the initial condition $b_2 = 2 \sin(2\pi x_1)$, a simple field having zero mean and an energy density of unity. The initial velocity is zero, and the forcing power is unity. The viscosity is 10^{-3} and the resistivity is 10^{-4} (identical to simulation A4). The magnetic field

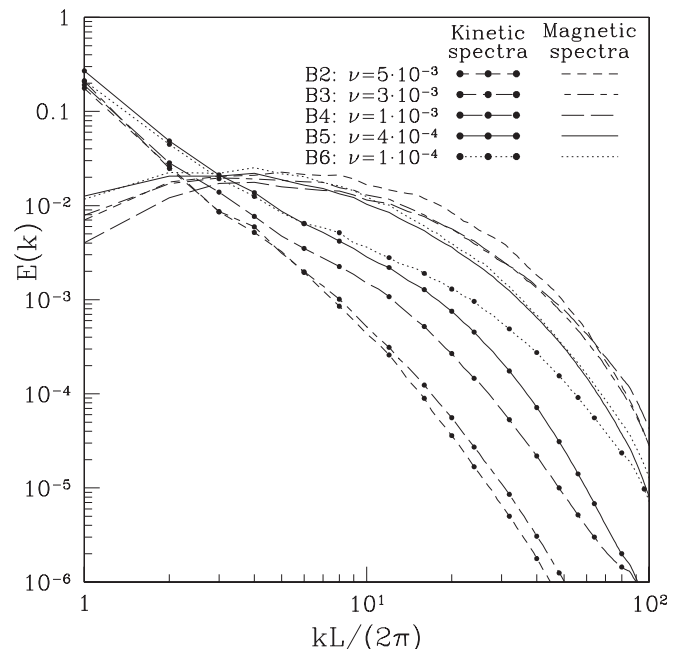


FIG. 13.—Same arrangement as for Fig. 12, although here with the 256^3 simulations B2–B6 (Table 4). As before, the magnetic spectrum at fixed resistivity is largely independent of viscosity.

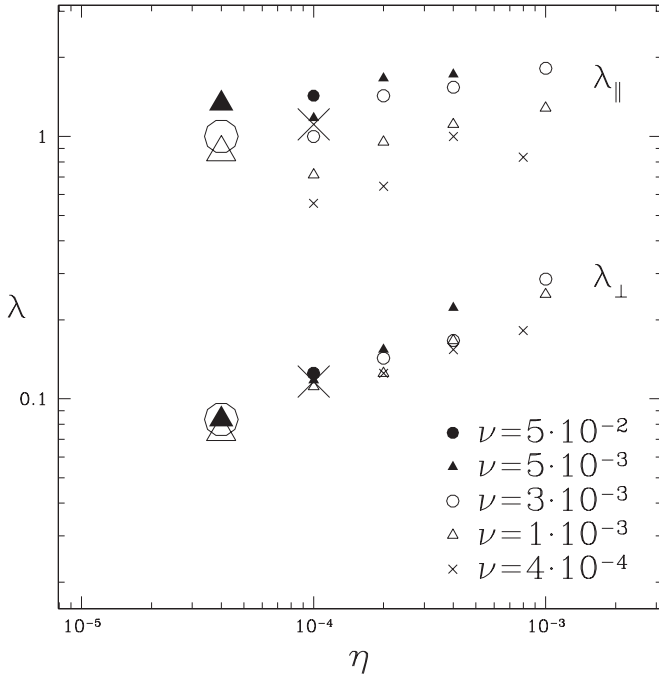


FIG. 14.—Longitudinal (*upper rows of symbols*) and transverse (*lower rows of symbols*) folding scales defined in eqs. (5) and (6). These numbers come from the saturated states of simulations for a range of values in ν and η . Small symbols represent 128^3 simulations, and large symbols represent 256^3 simulations.

evolves to the saturated state A4 after approximately 5 time units (Fig. 16). This initial condition is somewhat special as field lines can be interchanged and mixed (making the spacial scale smaller) without bending the lines.

The behavior with a strong mean field, $\langle B \rangle^2 > \langle V^2 \rangle$, is quite different from these two simulations. The mean component of the field remains exactly constant in the simulations. The spectrum of turbulence in such a field is known to be monotonically decreasing with k ; in fact, $E_v(k) \sim k^{-1.5}$ (Maron & Goldreich 2001). We speculate that for $\langle B \rangle^2 \ll \langle V^2 \rangle$, the saturated equilibrium state is (as our two examples indicate) independent of the initial conditions. The timescale for achieving the saturated state may be long for very strong large-scale fields.

5.5. Magnetic Structure and Unwinding Flows

The reduced magnetic tension of the saturated state was previously diagnosed by noting that $\lambda_{\parallel} / \lambda_{\perp} \gg 1$. A more direct test can be constructed by observing how fast magnetic tension generates kinetic energy. This is done by artificially setting the velocity to zero and observing the release of tension in the subsequent evolution. Specifically, we observe the new kinetic energy generated from field-line unwinding and where in Fourier space it appears. Folded field lines have less tension per energy than structureless field lines and hence unwind more slowly, generating less velocity. A random-phase field is generated from a structured field by randomizing the Fourier component orientations while preserving the power spectrum. The random-phase magnetic field serves as a reference for structureless field lines with a folding factor of about unity.

We draw from the nonlinearly saturated state of simulation A4 at $t = 12$ to initialize two test simulations. In simulation U4, we erased the velocity and restarted with the same viscosity. The resistivity was reduced to 10^{-5} to remove the effect of resistive magnetic energy loss. In simulation U4r we additionally randomize the phases of the magnetic Fourier modes. By com-

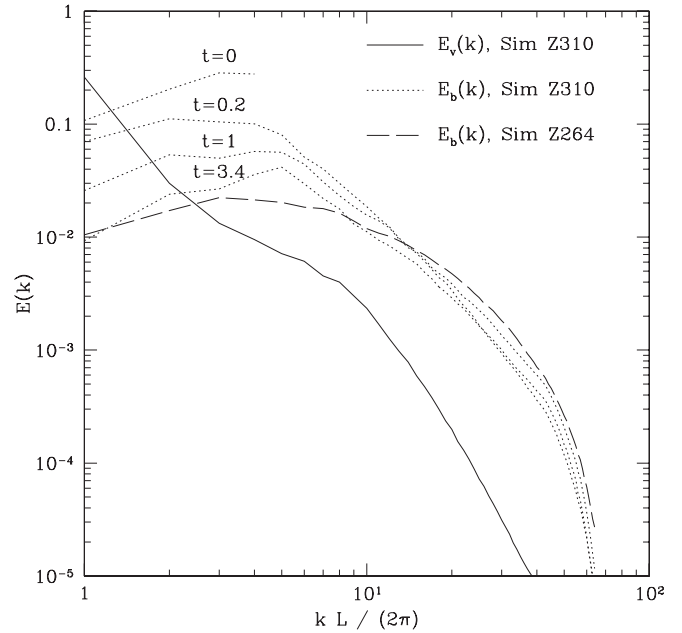


FIG. 15.—This figure follows the evolution of an initially large magnetic field at low k (simulation L3), until it reaches a state where the magnetic energy is dominantly at high k . The dashed line is the time-averaged saturated state of simulation A3, which has the same viscosity and resistivity.

paring the kinetic spectra generated in simulations U4 and U4r, we illustrate the effect of folding present in U4. We find that the structured magnetic field generates less velocity (particularly at early times) than the random-phase field, verifying that it has reduced tension per energy (Figs. 17 and 18). We also observe that the folded small-scale magnetic field generates large-scale velocity, while the random-phase field generates small-scale velocity. Specifically, the original magnetic field at $s \sim 15$ generates velocities at $s \sim 3$, while the random-phase field generates them at $s \sim 15$. We infer that for the dynamics of the

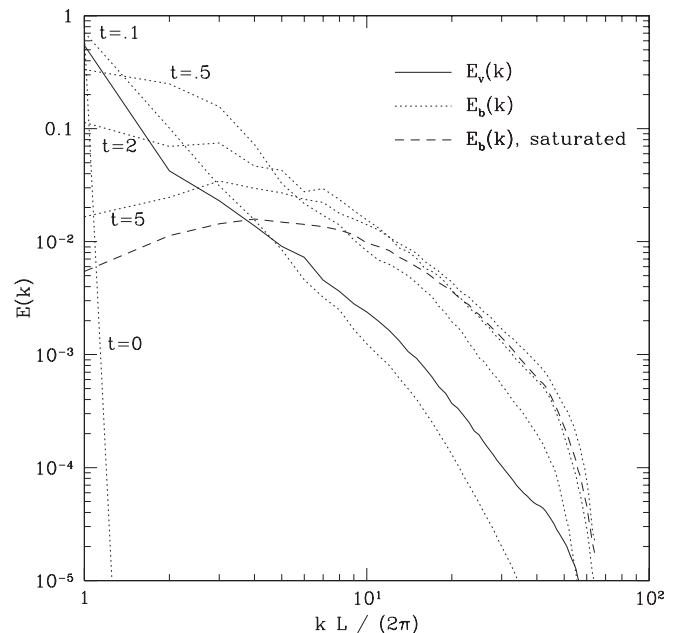


FIG. 16.—This figure follows simulation L4, which is similar to L3 except that the initial field is at even lower k . The dashed line is the time-averaged saturated state of simulation A4, which has the same viscosity and resistivity.

saturated state, only large-scale shear is responsible for the magnetic cascade, even though the kinetic spectrum is more shallow than k^{-3} . The cascade consists of a spectrally nonlocal interaction between large-scale velocities and small-scale magnetic fields. Therefore, the cascade proceeds according to one timescale, the forcing timescale. This also supports our claim that magnetic forces oppose shear that is less energetic than the magnetic field. Finally, the absence of production of kinetic energy beyond $s = 6$ (in the folded field-line case) establishes that unwinding of the small-scale field is unimportant.

5.6. Forcing Scale

Simulation K4 is forced at $3 \leq s \leq 4$, unlike the other simulations, which are forced at $1 \leq s \leq 2$. The initial conditions are taken from the saturated state of simulation A4. The viscosity and resistivity are the same as for simulation A4. The purpose is to determine if magnetic energy can occupy modes larger than the forcing scale. The result from Figure 19 is that they do not. Indeed the magnetic field for $1 \leq s \leq 2$ decays.

6. CONCLUSIONS

We began this paper by discussing a possible scenario for magnetic field growth in galaxies and to a lesser extent protogalaxies. The three stages of growth in the Galactic scenario are described in the introduction. However, the focus of this paper is on an idealized problem, the growth of field in homogeneous isotropic high magnetic Prandtl number turbulence. We argued that this problem is important to the early stages of growth in our Galactic scenario and to any protogalactic scenario. A series of computer simulations of this problem were performed. These simulations have yielded a qualitative picture (see § 2) of the growth and saturation of magnetic field. It is not clear how these results change our understanding of the origin of Galactic or protogalactic fields. What *is* clear is that the saturated state is dominated by small-scale fields that do not resemble either Galactic fields (Beck

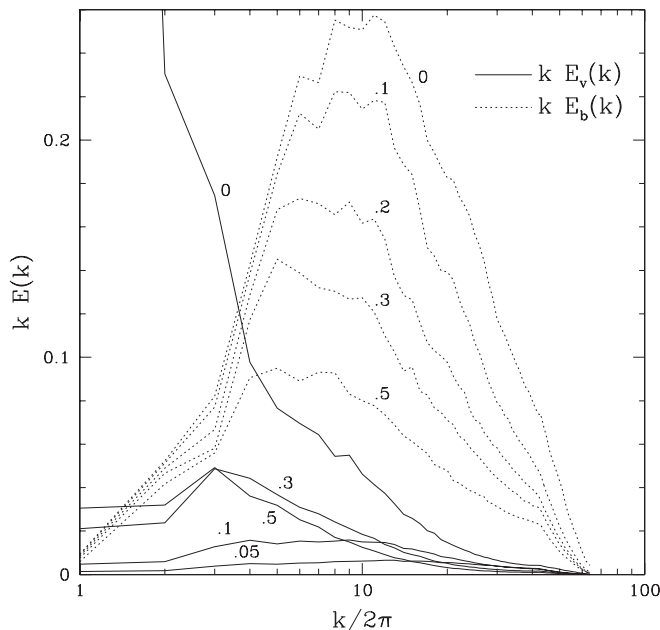


FIG. 17.—Simulation U4 started with a saturated magnetic spectrum in the folded state with the velocity set to zero. The $t = 0$ line corresponds to the velocity spectrum just before the velocity is set to zero. Subsequent evolution (numbers indicate times) without forcing generates large-scale velocities.

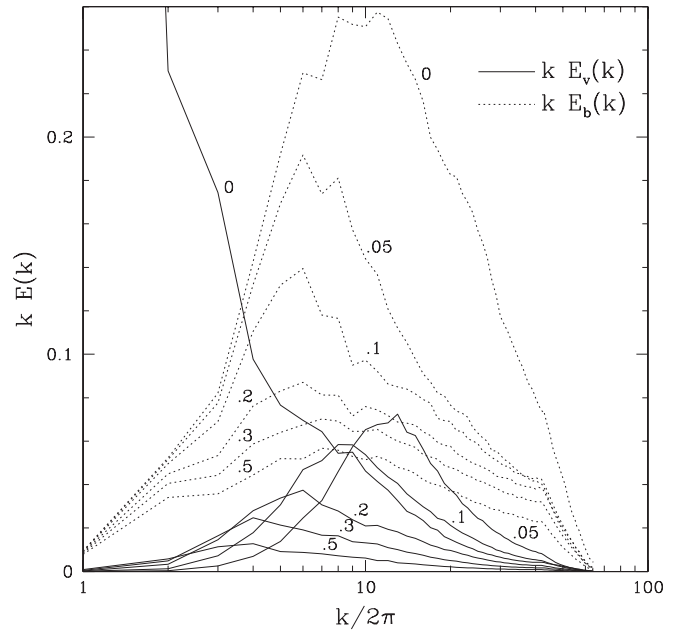


FIG. 18.—Simulation U4r started with the same saturated magnetic spectrum as simulation U4 in Fig. 17, but with randomized orientations of the magnetic Fourier modes. Subsequent evolution generates small-scale velocities, as opposed to the large-scale velocities from simulation U4. These simulations are discussed in § 5.5.

et al. 1996), where the fluctuating and mean (large-scale) fields are comparable, or cluster fields (Carilli & Taylor 2002), where the coherence length of the observed field is many kiloparsecs and therefore much larger than the resistive scale.

Let us review briefly the qualitative picture of growth and saturation. A weak seed field grows rapidly as a result of the stretching of viscous-scale eddies (see § 4). The spectrum of this weak field resembles the kinematic spectrum of Kulsrud and Anderson; specifically, it peaks at resistive scales and above these scales increases as $k^{3/2}$. The field is in a folded

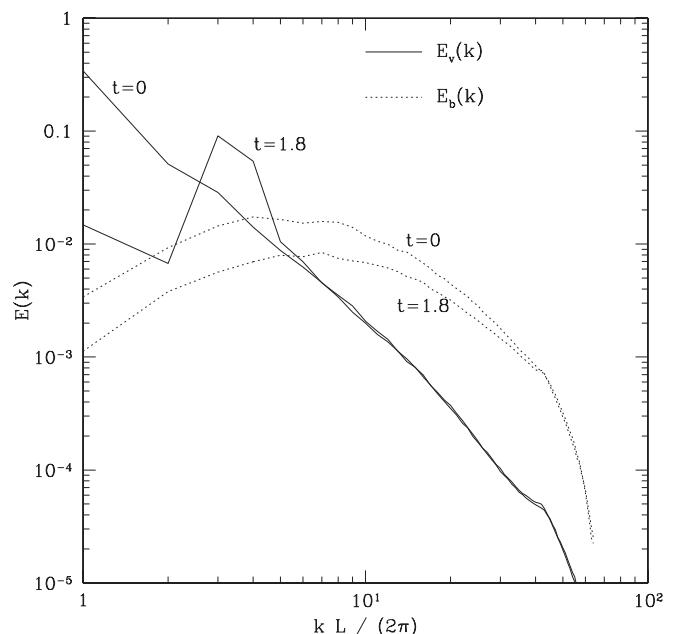


FIG. 19.—Simulation K4, forced at $3 \leq s \leq 4$ and initialized with the saturated state of A4. Magnetic energy in modes with $1 \leq s \leq 2$ decays.

“reduced-tension” state where $\mathbf{B} \cdot \nabla \mathbf{B} \sim B^2/l_v \ll \nabla B^2 \sim B^2/l_\eta$. The growth slows when the magnetic energy exceeds the kinetic energy in viscous-scale eddies. The field, at any instant, grows at the eddy turnover rate of the shearing scale. The shearing scale is defined to be the scale at which the total magnetic energy equals the kinetic energy in the shearing-scale eddies. Growth continues until the magnetic energy equals the kinetic energy in the stirring (largest) scale eddies. In the saturated state (§ 5) the magnetic energy remains equal to the total kinetic energy. The saturated spectrum peaks at the resistive scale associated with the stirring timescales, which, although it is larger than the resistive scale associated with the viscous timescale, is still small. The stirring-scale motions continue to stretch the field: this stretching is balanced by resistive destruction of field at the resistive scale. The saturated field is also in a folded reduced-tension state with $\mathbf{B} \cdot \nabla \mathbf{B} \sim B^2/l_f \ll \nabla B^2 \sim B^2/l_\eta$. There is little evidence in our simulations for a long time evolution of the magnetic spectrum (such as we postulated in Schekochihin et al. 2002a), where resistivity removes the smaller scales, allowing the larger scales to grow and become progressively more dominant.

We have performed additional simulations to test various aspects of the qualitative scenario. Two simulations were initialized with strong (equipartition) large-scale fields (see § 5.4). These simulations evolved to the same small-scale field dominated state obtained from weak initial fields. To demonstrate how the folded reduced-tension state of the field drives very little unwinding flows, we compared unwinding flows in the

true folded field and in a field with the same spectrum but randomized phases (see § 5.5). The folded field drove large-scale but no small-scale flows and the random-phase field drove strong small-scale flows.

It is clear that a proper understanding of the growth and saturation of magnetic field in galaxies requires treating the full geometric complexities of the disk and halo. This has been recognized from the earliest discussions of Galactic dynamos (Parker 1979). We are starting to perform simulations of Galactic disks. Such simulations can at best probe the large-scale field dynamics. The dynamics investigated in this paper, specifically the generation of small-scale fields, will affect the large-scale field generation. Realistic inclusion of this interaction is not possible computationally, and further understanding of the idealized problem discussed here is still needed.

We wish to thank Alex Schekochihin, Greg Hammett, Benjamin Chandran, Eric Blackman, Ellen Zweibel, Yoram Lithwick, George Field, Axel Brandenburg, Russell Kulsrud, Bill Matthews, and Annick Pouquet for helpful discussions. We benefited from the supercomputers at the Caltech Center for Advanced Computing Resources and at the National Center for Supercomputing Applications at UIUC and from their very helpful staff. This work was supported by EPSRC grant GR/R55344/01 and NSF grant AST 00-98670.

APPENDIX A

INDEX OF SIMULATIONS

Table 4 provides an index of simulations.

TABLE 4
INDEX OF SIMULATIONS

ID	Grid	ν	η	Pr	Notes
A0.....	128^3	5×10^{-2}	0	...	
A1.....	128^3	5×10^{-2}	2×10^{-5}	2500	
A2.....	128^3	5×10^{-3}	1×10^{-4}	50	
A3.....	128^3	3×10^{-3}	1×10^{-4}	30	
A4.....	128^3	1×10^{-3}	1×10^{-4}	10	
A5.....	128^3	4×10^{-4}	4×10^{-4}	1	
B1.....	256^3	5×10^{-2}	1×10^{-5}	5000	
B2.....	256^3	5×10^{-3}	4×10^{-5}	125	
B3.....	256^3	3×10^{-3}	4×10^{-5}	75	
B4.....	256^3	1×10^{-3}	4×10^{-5}	25	
B5.....	256^3	4×10^{-4}	1×10^{-4}	4	
B6.....	256^3	1×10^{-4}	1×10^{-4}	1	
L3.....	128^3	3×10^{-3}	1×10^{-4}	1	Initial \mathbf{B} at $k = 4$ with large energy
L4.....	128^3	1×10^{-4}	1×10^{-4}	1	Initial \mathbf{B} at $k = 1$ with large energy
U4.....	128^3	$1 \times 10^{-3*}$	1×10^{-5}	100	Erase \mathbf{v} from A4 and continue
U4r.....	128^3	$1 \times 10^{-3*}$	1×10^{-5}	100	Like U4, and with random-phased \mathbf{B}
K4.....	128^3	1×10^{-3}	1×10^{-4}	100	Force at $s = 3$ and 4
A4w.....	128^3	1×10^{-3}	1×10^{-6}	1000	Start from weak field
A5w.....	128^3	4×10^{-4}	1×10^{-6}	1000	Start from weak field
A4s.....	128^3	1×10^{-3}	1×10^{-6}	1000	Start from saturated state of A4
A5s.....	128^3	4×10^{-4}	1×10^{-6}	1000	Start from saturated state of A5
S1.....	128^3	1×10^{-3}	1×10^{-3}	1	
S2.....	128^3	4×10^{-4}	1×10^{-3}	0.4	
S3.....	128^3	4×10^{-4}	2×10^{-3}	0.2	
S4.....	128^3	4×10^{-4}	4×10^{-3}	0.1	

NOTES.—The following properties are common to all simulations: the box size is (1, 1, 1), and the kinetic energy is forced with a power of unity. Forcing occurs within a sphere of radius 2 in Fourier lattice space, except for simulation K4, which is forced at a radius of 3 and 4.

APPENDIX B

RESOLUTION

The important folded structure is absent in simulations where insufficient resistivity is used. This is because when the resistivity is small enough the spectral procedure indirectly contributes to magnetic energy loss. Although the nonlinear terms in a properly dealiased pseudospectral algorithm conserve total energy summed over all resolved Fourier modes, there can still be other kinds of errors. In particular, the loss of interactions with unresolved modes can alter the phase relationships between modes, thereby destroying folded field-line structure and increasing the magnetic tension per unit energy. We find that 128^3 simulations require $\eta > 10^{-4}$ and 256^3 simulations require $\eta > 3 \times 10^{-5}$. In this appendix we examine the consequences of insufficient resistivity.

When η is lowered below the resolution limit, λ_{\perp} becomes as expected independent of η and λ_{\parallel} decreases markedly. The folded structure is at least partially destroyed. This can also be seen in the spectrum of $\mathbf{B} \cdot \nabla \mathbf{B}$, the tension spectrum. In Figure 20 we plot the tension spectrum for two resistivities, A4 with $\eta = 10^{-4}$ and A4w with $\eta = 10^{-6}$. A4w has insufficient resistivity and the small-scale tension is enhanced over the A4, which has sufficient resistivity (but barely so). It is interesting that the tension spectrum of A4 is roughly flat. The tension spectrum after the phases (of A4) are randomized is also plotted in Figure 20; this spectrum peaks at the smallest scales. The tension spectrum of the underresolved case, A4w, is closer to the random-phase spectrum than the resolved case.

The extra magnetic tension forces in the underresolved case generate unwinding velocities that dissipate viscously and remove magnetic energy by unwinding. Thus, in simulations with insufficient resistivity, viscous dissipation near the dealiasing cutoff becomes significant. In a sense viscosity takes over the energy dissipation role of resistivity, diminishing the effect of lowering the resistivity in simulation A4s.

Although not obvious in the spectra, this effect can be seen by plotting the viscous and resistive dissipation. In Figure 21 we plot the energy and dissipation of simulations A4 ($\nu = 10^{-3}$, $\eta = 10^{-4}$) and A4t ($\nu = 10^{-3}$, $\eta = 3 \times 10^{-5}$). Lowering the resistivity by a factor of 3.3 in simulation A4t does not significantly change the magnetic energy spectrum. However, viscous dissipation of dealiasing scale unwinding velocities dominates the dissipation in A4t. In contrast, dissipation in A4 is roughly half viscous dissipation at the viscous scale and half resistive dissipation at the resistive scale. Clearly, A4t is underresolved: even A4 has slightly too little resistivity as can be seen from the structure at the resistive scale.

APPENDIX C

SPANDEX WAVES

MHD interactions exist that are nonlocal in k space. For instance, large-scale shear can transfer energy directly to small-scale magnetic fields. Alfvén waves are an oscillatory phenomenon where small-scale perturbations interact with a uniform magnetic field. A similar oscillatory phenomenon exists in a tangled magnetic field. Here a large-scale velocity perturbation generates a

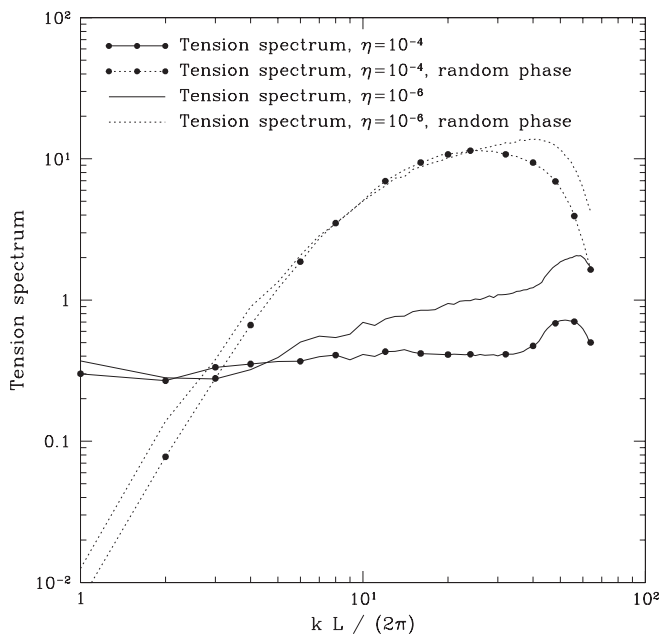


FIG. 20.—We plot the spectrum of the tension term, $\mathbf{B} \cdot \nabla \mathbf{B}$, to show the effect of lowering the resistivity enough so that aliasing destroys folding structure and enhances tension. The simulations are A4 and A4w, which both have $\nu = 10^{-3}$. A4 has a resistivity of 10^{-4} , and A4w has a resistivity of 10^{-6} . The random-phase spectra are also shown for comparison.

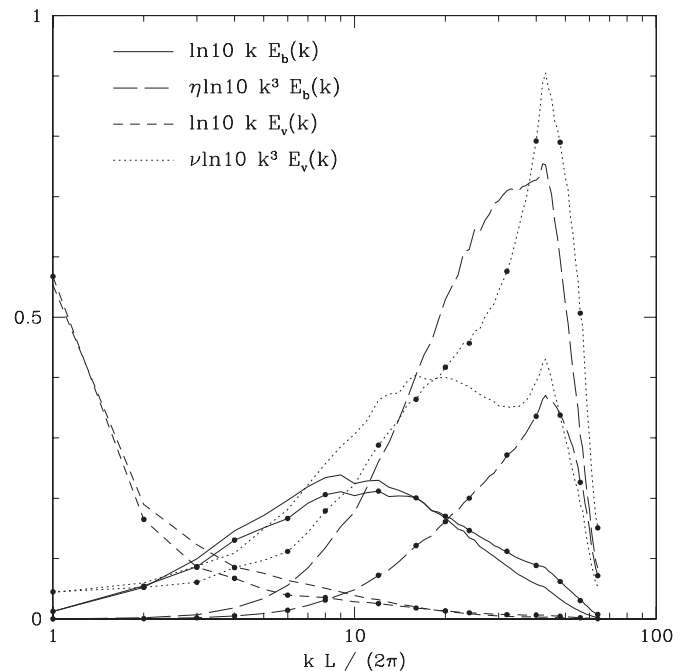


FIG. 21.—Lines without circles denote simulation A4 with $\eta = 10^{-4}$, and lines with circles denote simulation A4t with $\eta = 3 \times 10^{-5}$. In simulation A4t, dealiasing destroys folded magnetic structure and increases magnetic tension, resulting in small-scale unwinding velocities and viscous dissipation.

back-reaction in a small-scale tangled field. Locally, magnetic forces act in all directions, but spatially averaged, they tend to act collectively to oppose the original large-scale perturbation.

Define a Lagrangian displacement field $\zeta = \hat{\mathbf{a}}e^{i(\mathbf{k} \cdot \mathbf{x} - \omega t)}$, with $\mathbf{k} \cdot \hat{\mathbf{a}} = 0$ and $\mathbf{v} = d_t \zeta$. Let $\mathbf{B} = \mathbf{B}_0 + \hat{\mathbf{a}}(\mathbf{B}_0 \cdot \mathbf{k})ie^{i(\mathbf{k} \cdot \mathbf{x} - \omega t)}$, where \mathbf{B}_0 is the static nonoscillatory part with an assumed scale of much less than k^{-1} . Any other time evolution in \mathbf{v} and \mathbf{B} is neglected, as well as viscosity and resistivity. \mathbf{B} satisfies the induction equation $\mathbf{B} = \int d_t \mathbf{B} dt = \mathbf{B} \cdot \nabla \zeta$. Returning to the Navier-Stokes equation, $\langle d_t \mathbf{v} \rangle = -\omega^2 e^{i(\mathbf{k} \cdot \mathbf{x} - \omega t)} = \langle \mathbf{B} \cdot \nabla \mathbf{B} \rangle = \langle \mathbf{B}_0 \cdot \nabla \mathbf{B}_0 \rangle - \langle (\mathbf{B}_0 \cdot \mathbf{k})^2 \rangle e^{i(\mathbf{k} \cdot \mathbf{x} - \omega t)}$. An average is taken over scale k , which implies $\langle \mathbf{B}_0 \cdot \nabla \mathbf{B}_0 \rangle \sim 0$ and $\langle (\mathbf{B}_0 \cdot \mathbf{k})^2 \rangle \sim \langle (\mathbf{B}_0)^2 \rangle k^2/3$. Here ζ has an oscillatory eigenmode with phase speed $\langle (\mathbf{B}_0)^2/3 \rangle^{1/2}$. This is equivalent to the Alfvén speed if we only consider the averaged magnetic field component along \mathbf{k} .

REFERENCES

- Batchelor, G. K. 1950, Proc. R. Soc. London A, 201, 405
 Beck, R., Brandenburg, A., Moss, D., Shukurov, A., & Sokoloff, D. 1996, ARA&A, 34, 155
 Bhattacharjee, A., & Yuan, Y. 1995, ApJ, 449, 739
 Blackman, E. G., & Field, G. B. 2000, ApJ, 534, 984
 ———. 2002, Phys. Rev. Lett., 89, 265007
 Braginskii, S. I. 1965, Rev. Plasma Phys., 1, 205
 Brandenburg, A. 2001, ApJ, 550, 824
 Carilli, C., & Taylor, G. 2002, ARA&A, 40, 319
 Cattaneo, F., & Hughes, D. W. 1996, Phys. Rev. E, 54, 4532
 Chertkov, M., Falkovich, G., Kolokolov, I., & Lebedev, V. 1999, Phys. Rev. Lett., 83, 4065
 Cho, J., & Vishniac, E. 2000a, ApJ, 538, 217
 ———. 2000b, ApJ, 539, 273
 Field, G. B., & Blackman, E. G. 2002, ApJ, 572, 685
 Field, G. B., Blackman, E. G., & Chou, H. 1999, ApJ, 513, 638
 Glatzmaier, G. A., & Roberts, P. H. 1995, Nature, 377, 203
 Gnedin, N., Ferrara, A., & Zweibel, E. G. 2000, ApJ, 539, 505
 Gruzinov, A., Cowley, S., & Sudan, R. 1996, Phys. Rev. Lett., 77, 4342
 Gruzinov, A., & Diamond, P. 1994, Phys. Rev. Lett., 72, 1651
 Kazantsev, A. P. 1968, Soviet Phys.—JETP Lett., 26, 1031
 Kinney, R. M., Chandran, B., Cowley, S., & McWilliams, J. C. 2000, ApJ, 545, 907
 Kinney, R. M., & McWilliams, J. C. 1998, Phys. Rev. E, 57, 7111
 Kolmogorov, A. N. 1941, Dokl. Akad. Nauk SSSR, 30, 9
 Kronberg, P. 1994, Rep. Prog. Phys., 59, 325
 Kulsrud, R. M. 1999, ARA&A, 37, 37
 Kulsrud, R. M., & Anderson, S. W. 1992, ApJ, 396, 606
 Lithwick, Y., & Goldreich, P. 2001, ApJ, 562, 279
 Malyszhkin, L. M., & Kulsrud, R. M. 2002, ApJ, 571, 619
 Maron, J. 2000, Ph.D. thesis, Caltech
 Maron, J., & Blackman, E. 2002, ApJ, 566, L41
 Maron, J., & Goldreich, P. 2001, ApJ, 554, 1175
 Meneguzzi, M., Frisch, U., & Pouquet, A. 1981, Phys. Rev. Lett., 47, 1060
 Mestel, L. 1999, Stellar Magnetism (Oxford: Oxford Univ. Press)
 Moffatt, H. K. 1978, Magnetic Field Generation in Electrically Conducting Fluids (Cambridge: Cambridge Univ. Press)
 Muller, W., & Biskamp, D. 2000, Phys. Rev. Lett., 84, 475
 Parker, E. N. 1979, Cosmical Magnetic Fields (Oxford: Oxford Univ. Press)
 Pouquet, A., Frisch, U., & Leorat, J. 1976, J. Fluid Mech., 77, 321
 Ruzmaikin, A. A., Shukurov, A. M., & Sokoloff, D. D. 1988, Magnetic Fields of Galaxies (Dordrecht: Kluwer)
 Schekochihin, A. A., Boldyrev, S. A., & Kulsrud, R. M. 2002a, ApJ, 567, 828
 Schekochihin, A. A., Cowley, S., Maron, J., Hammett, G. W., & McWilliams, J. C. 2002b, New J. Phys., 4, 84
 Schekochihin, A. A., Cowley, S., Maron, J., & Malyszhkin, L. 2002c, Phys. Rev. E, 65, 016305
 Schekochihin, A. A., Maron, J., Cowley, S., & McWilliams, J. 2002d, ApJ, 576, 806
 Taylor, G. B., Allen, S. W., & Fabian, A. C. 1999, in Diffuse Thermal and Relativistic Plasma in Galaxy Clusters, ed. H. Bohringer, L. Feretti, & P. Schuecker (Garching: MPE), 77
 Valsecchi, J. P. 1998, Fundam. Cosmic Phys., 19, 319
 Zel'dovich, Ya. B. 1957, Soviet Phys.—JETP Lett., 4, 460
 Zweibel, E. G., & Brandenburg, A. 1997, ApJ, 478, 563
 Zweibel, E. G., & Heiles, C. 1997, Nature, 385, 131